SUB-NYQUIST ACQUISITION HARDWARE FOR WIDEBAND COMMUNICATION

Moshe Mishali, Yonina C. Eldar, Oleg Dounaevsky and Eli Shoshan

Department of Electrical Engineering
Technion — Israel Institute of Technology, Haifa, Israel
{moshiko@tx, yonina@ee, doleg@ee, elis@ee}.technion.ac.il

ABSTRACT

We present a sub-Nyquist analog-to-digital converter of wideband inputs. Our circuit realizes the recently proposed modulated wideband converter, which is a flexible platform for sampling signals according to their actual bandwidth occupation. The theoretical work enables, for example, a sub-Nyquist wideband communication receiver, which has no prior information on the transmitter carrier positions. Our design supports input signals with 2 GHz Nyquist rate and 120 MHz spectrum occupancy, with arbitrary transmission frequencies. The sampling rate is as low as 280 MHz. To the best of our knowledge, this is the first reported wideband hardware for sub-Nyquist conversion. We describe the various circuit design considerations, with an emphasis on the nonordinary challenges the converter introduces: mixing a signal with a multiple set of sinusoids, rather than a single local oscillator, and generation of highly-transient periodic waveforms, with transient intervals on the order of the Nyquist rate. Hardware experiments validate the design and demonstrate sub-Nyquist sampling and signal reconstruction.

Index Terms— Analog to digital conversion, circuit implementation, modulated wideband converter, sub-Nyquist sampling, wideband communication, Xampling.

1. INTRODUCTION

Analog to digital conversion (ADC) is the key enabling many of the advances in signal processing. The common practice for ADC in wideband communication is demodulation, namely multiplying the input by the carrier frequency f_c of a band of interest, so as to shift the contents of the narrowband transmission from the high frequencies to the origin. Then, commercial ADC devices at low rates are utilized. Demodulation, however, requires knowing the exact carrier frequency. To-date, the alternative to demodulation is to sample the entire wideband spectrum, or to use nonuniform sampling strategies which effectively require an ADC device with Nyquist-rate front-end bandwidth [1, 2].

In this paper, we present a circuit-level hardware prototype of a sub-Nyquist sampling system, realizing the modulated wideband converter (MWC) strategy of [1]. The MWC can sample wideband inputs at a low rate, proportional to the actual bandwidth occupation, without knowledge of the carrier positions. Theoretical background and the specifications we realize in hardware are detailed in Section 2. The MWC strategy involves mixing the signal with highly-transient periodic waveforms, then lowpass filtering a narrow working band followed by standard lowrate ADCs. To the best of our knowledge, based on [2] and the discussion on related work herein, our system is the first wideband hardware achieving minimal sub-Nyquist rates without knowledge of the carrier positions.

M. Mishali is supported by the Adams Fellowship Program of the Israel Academy of Sciences and Humanities.

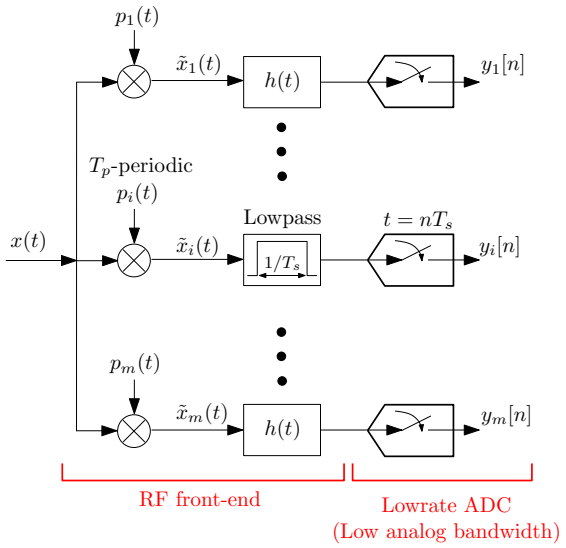

Fig. 1: The modulated wideband converter: a practical sub-Nyquist sampling system for multiband signals.

Sections 3 and 4 elaborate on the circuit challenges we encountered while developing the hardware. The essence of this circuit work is that nonordinary and tricky, yet simple, design techniques materialize the mathematical ideas. To verify the design, a sub-Nyquist sampling and reconstruction demonstration is presented in Section 5. Documentation and video recordings are available online [3].

2. MODULATED WIDEBAND CONVERTER

2.1. Theoretical background

The MWC is aimed at sampling wideband sparse signals at sub-Nyquist rates according to the scheme of Fig. 1. To accomplish the goal, a multiband input model is assumed. An analog signal $x(t)$ is termed multiband if its Fourier transform $X(f)$ is concentrated on N frequency intervals, or bands, such that the individual bandwidths are not greater than B Hz. An illustration of multiband spectra appears in Fig. 2. The maximal possible frequency of $x(t)$, denoted by $f_{\max}$, dictates the Nyquist rate

$$f_{\text{NYQ}} = 2f_{\max}. \tag{1}$$

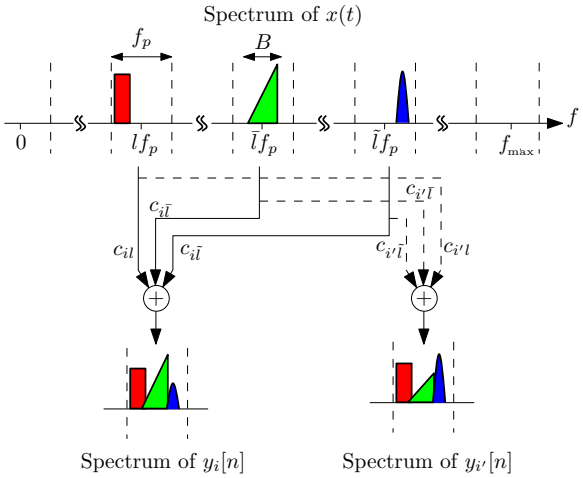

Fig. 2: The spectrum slices from $x(t)$ are overlayed in the spectrum of the output sequences $y_i[n]$. In the example, channels i and i' realize different linear combinations of the spectrum slices centered around $lf_p, \bar{l}f_p, \tilde{l}f_p$. For simplicity, the aliasing of the negative frequencies is not drawn.

The values of N, B, f_{max} depend on the specifications of the application at hand, such as the expected number of concurrent transmissions and the communication technology which defines the narrowband widths. The multiband model does not assume knowledge of the carrier locations f_i, and these can lie anywhere below f_{max}.

The analog front-end of the MWC preprocesses an analog multiband signal as follows. A wideband signal $x(t)$ enters m channels simultaneously. In the ith channel the signal is multiplied by a periodic function $p_i(t)$ with period $T_p = 1/f_p$. The product is lowpass filtered by $h(t)$ with cutoff $f_s/2$, and then sampled uniformly every $T_s = 1/f_s$ seconds.

The mixing operation scrambles the spectrum of $x(t)$, such that a portion of the energy of all bands appears in baseband. More specifically, since each $p_i(t)$ is periodic, it has a Fourier expansion

$$p_i(t) = \sum_{l=-\infty}^{\infty} c_{il} e^{j\frac{2\pi}{T_p} lt}. \tag{2}$$

Therefore, the mixing results in a weighted-sum of f_p-shifted copies of $X(f)$, such that the weights are the Fourier coefficients c_{il} [1]. The lowpass filter $h(t)$ transfers only the narrow band frequencies up to $f_s/2$ from that mixture to the output sequence $y_i[n]$. The aliased output is illustrated in Fig. 2. Whilst aliasing is often an undesired artifact in sampling, here it is deliberately utilized to generate mixtures at baseband. Intuitively, if $p_i(t)$ are wisely designed to capture different mixtures of the spectrum, then the input $x(t)$ is determined from the samples $y_i[n]$, $1 \le i \le m$. The exact parameter values and periodic waveforms are specified below.

Lowrate ADCs follow the RF front-end. Commercial devices can be used for that task due to the preceding lowpass. The fact that the ADCs see only a lowpass input is a major advantage over classic nonuniform methods [4, 5] which acquire pointwise values of $x(t)$, and therefore necessitate an ADC with Nyquist-rate track-and-hold circuitry. In contrast, the MWC shifts the Nyquist burden to RF technology, thereby avoiding interaction of wideband signals with the ADC devices. We also point out that [4, 5] assume the band positions, while the MWC setup does not require this knowledge.

Table 1: Prototype specifications

Parameter	Choice
Signal model	$N = 6$, $B = 19$ MHz, $f_{\text{NYQ}} = 2$ GHz
Number of channels m	4
Waveform type	periodic sign alternation
Alternation rate	2.075 GHz
Sign pattern length M	108
Period f_p	$2.075/108 = 19.212$ MHz
Filter cutoff	33 MHz
Sampling rate/channel f_s	70 MHz

2.2. Hardware specifications

The MWC is a flexible system with various parameters, of which we chose to realize the specifications that appear in Table 1. We next motivate these choices.

The multiband model matches a scenario of 3 concurrent transmissions in the setup that was numerically simulated in [1]. The Nyquist rate $f_{\text{NYQ}} = 2.075$ GHz stems from the frequency of a voltage-controlled-oscillator (VCO) in our system and can be increased for higher VCO frequencies.

The basic parameter choice that is described in [1] is $m \ge 4N$ and $f_s = f_p \ge B$. This choice results in a sampling rate of $4NB$, which can be significantly smaller than f_{NYQ}. The basic choice implies $m = 4N = 24$ sampling branches. In order to save hardware size and price, we utilized an advanced MWC version, also proposed in [1], in which the number of physical channels is collapsed by a factor of q, at the expense of increasing the sampling rate of each channel by the same factor, so that $f_s = qf_p$. Our design uses a collapsing factor $q = 3$. To further reduce m, an extra factor of 2 is accomplished by combining digital techniques from [6] in the reconstruction algorithm. Consequently, $m = 4N/q/2 = 4$ is the actual number of sampling branches.

We followed a suggestion of [1] and chose cyclic sign-alternating functions for $p_i(t)$. A theoretical study in [7] showed that popular binary patterns, *e.g.,* the Gold or Kasami sequences that are widely used in communication for their low mutual correlation, fit the MWC system [7]. In practice, we designed a single shift-register (SR) with 2 GHz clock rate, and tapped the register at four locations, so that $p_i(t)$ are delayed versions of a single binary pattern. This choice reduces the hardware size and was also suggested in [1]. Section 4 explains how we initialize the SR.

Our prototype implements the RF front-end of the MWC using two physical boards. An analog board realizes the four analog paths from $x(t)$ to the relevant filter outputs, whereas a digital counterpart provides the periodic waveforms. This hardware scope captures the innovative theoretical parts as well as the challenges in the actual design, which are explained in the sequel. The filter cutoff of 33 MHz allows a sampling rate of $f_s = 70$ MHz. In our lab experiments, a 4-channel scope is used for digitizing the $m = 4$ filter outputs. Future work will embed commercial ADC devices for that task; relevant devices with 16 bits resolution include AD9460 and ADS5562. The 33 MHz cutoff is slightly higher than half of the working band, $qf_p/2 = 28.8$ MHz, to allow flat phase response over the passband. Nonideal amplitude response is calibrated after manufacturing [8].

We note that the theory of multiband sampling necessitates a minimal sampling rate of $2NB = 228$ MHz, regardless of the sampling architecture [6]. Our realization approaches the bound with

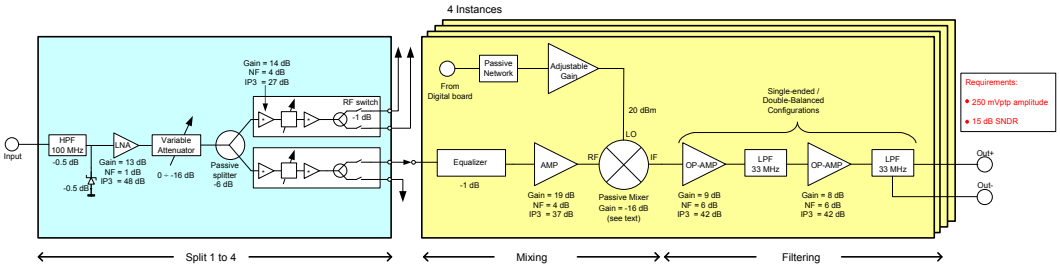

Fig. 3: A block diagram of the analog board.

$4f_s = 280$ MHz sampling rate, that is about 14% of the Nyquist rate.

2.3. Circuit challenges

In designing an analog circuit to realize the MWC we encountered two main show-stoppers: (I) analog mixing with spectrally-rich waveforms $p_i(t)$, and (II) constructing the periodic waveforms with the required alternation speed of 2.075 GHz. RF mixers are tailored for multiplication with a single sinusoid, presumably for standard modulating and demodulating of an information band by its carrier f_c. In contrast, the MWC requires a simultaneous multiplication with many sinusoids – those comprising $p_i(t)$. This results in attenuation of the output and substantial nonlinear distortion not accounted for in datasheet specifications. The next section describes the way mixing with periodic waveforms is tackled in our design.

The second challenge pertains to constructing $p_i(t)$. The waveforms can be generated either by analog or digital means. Analog waveforms, such as sinusoid, square or sawtooth, are smooth within the period, and therefore do not have enough transients at high frequencies which is necessary to ensure sufficient aliasing. On the other hand, digital waveforms can be programmed to any desired number of alternations within the period, but require meeting timing constraints on the order of the clock period. In our setting, the clock interval of $1/f_{\text{NYQ}} = 480$ picosecs leads to severe timing constraints that are difficult to satisfy with existing digital devices. Section 4 elaborates on the solution we found for this challenge.

Our goal in the present paper is to focus on the hardware realization of the RF front-end of Fig. 1. Reconstruction of the signal is carried out digitally [1]. Section 5 briefly overviews the recovery algorithm and demonstrates signal reconstruction from sub-Nyquist sampling rate.

3. ANALOG BOARD

The analog board consists of three consecutive stages: splitting the input into four channels, mixing with a given set of periodic waveforms $p_i(t)$ and lowpass filtering. Fig. 3 presents a block diagram of the analog path end-to-end.

3.1. Dynamic range

In realizing our sub-Nyquist system, we bared in mind the representative application of a wideband receiver, which needs to amplify the input to a level that the ADC can treat. To design the RF path of Fig. 3, gains, noise figures, and third intersection-point (IP3) parameters of the devices along the path were used in order to calculate

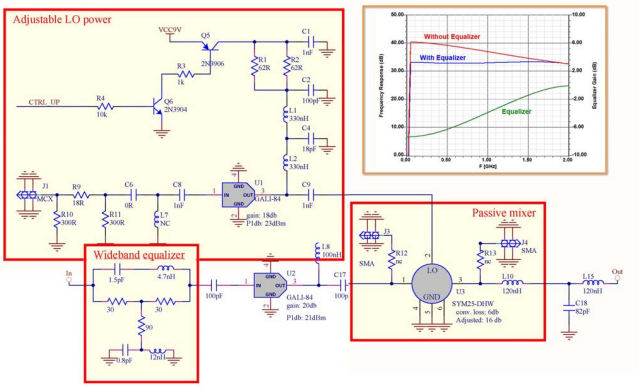

Fig. 4: Schematics of mixing with multiple sinusoids. The wideband equalizer flattens the frequency response at the RF port of the mixer. Low frequencies (up to 500 MHz) are attenuated by approximately 8 dB, whereas high frequencies (above 1.5 GHz) are not altered.

the amplitude and signal to noise ratio (SNR) at each output. The detailed calculations in the technical report [9] predict a dynamic range of 49 dB input power, which was validated experimentally.

In conducting the SNR analysis we encountered the first consequence of the nonordinary mixing – the datasheet specifications of commercial mixer devices do not cover the case of multiple harmonics at the local oscillator (LO) port. To predict the actual mixer's parameters, we had to perform our own lab evaluations for the chosen device, which led to the following adjustments

$$\begin{array}{lrlrl} \text{Loss:} & -16 & \text{dB} \rightarrow & -6 & \text{dB} \\ \text{IP3:} & 27 & \text{dBm} \rightarrow & 30 & \text{dBm} \\ \text{LO power:} & 17 & \text{dBm} \rightarrow & 20 & \text{dBm.} \end{array} \tag{3}$$

These modifications impact the components in the RF path, since without adjusting the datasheet values, conventional noise analysis would falsely indicate that a smaller gain is needed.

3.2. Mixing with multiple sinusoids

The key idea behind the MWC strategy is periodic mixing. The schematic of the mixing block, Fig. 4, highlights three additional impacts due to the nonordinary mixing with multiple sinusoids. A passive mixer was chosen since active ones typically allow a narrow range of LO frequencies, whereas $p_i(t)$ span a wide spectrum. The tunable power control on $p_i(t)$ was inserted to allow flexible post-manufacturing refinements of the datasheet adjustments (3). Such a

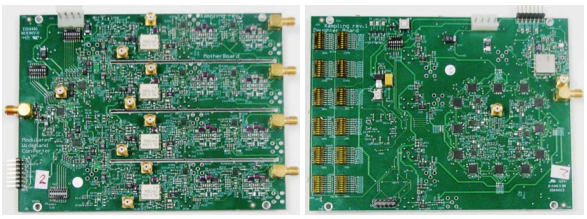

Fig. 5: The analog board (left-pane) realizes four sampling channels, including the amplification path, mixing with four input periodic waveforms (connectors on the rear), and lowpass filtering. The digital board (right-pane) provides four sign-alternating periodic waveforms of length $M = 108$, derived from different taps of a single shift-register.

power control is not needed in standard mixing for which datasheet guarantees the performance.

The third block in Fig. 4 is a wideband equalizer. The equalizer is located near the LO port, just before the mixer, instead of the common knowhow of equalization towards the end of the chain, near the ADC terminals or even in the digital domain, where it can flatten the response of the entire analog path. The reason is again the nonordinary mixing. More specifically, recall that conventional equalization corrects the effective system response

$$H_{\text{total}}(f) = \prod_i G_i(f - f_c) \prod_i H_i(f), \tag{4}$$

where $G_i(f), H_i(f)$ are the responses of the devices preceding and following the mixer, respectively. The shift in the $G_i(f)$ responses accounts for the effect of standard demodulation, in which $x(t)$ is multiplied by a single frequency source of f_c Hz. In contrast, our sub-Nyquist system produces the product $x(t)p_i(t)$ which contains a weighed-sum of f_p-wide spectrum slices of $x(t)$; see Fig. 2. Consequently, there is no simple way to translate the frequency response of the devices preceding the mixer, as in (4), to an equivalent response at the output. An analog equalizer, if located after the mixer, cannot be designed to flatten the response of the weighed-sum in $y_i[n]$. This explains why we placed the equalizer circuit before the mixer. Compensating for the rest of the path, namely for the nonideal response of the filter $h(t)$, is done digitally [8]. A circuit simulation of the equalizer is presented in the top-right corner of Fig. 4, ensuring an equalized flat response over the wideband regime until 2 GHz.

3.3. Lowpass filtering of spectrum mixtures

Lowpass filtering is the last step in the analog domain. The modern trend in engineering is to shift filtering tasks to a digital processor. Here, analog processing is inevitable, since the filter is responsible for reducing the signal bandwidth before entering the ADC.

In standard bandlimited sampling, a lowpass filter has the role of rejecting noise out of band. The noise is typically small and thus does not require a sharp cutoff. In the MWC prototype, the input to the filter contains energy spread all across the spectrum, with nonelligible power beyond the cutoff. For this reason, we realized a sharp cutoff around 33 MHz using two elliptic filters of order 7 concatenated and buffered, as visualized in Fig. 3.

A photo of the analog board is attached in Fig. 5. Table 2 lists the reference names of the devices in our system, allowing to reproduce the design in a standard electronic laboratory.

Table 2: Device list

	Device	Reference	Manufacturer
Analog board	LNA	SPF5043	RFMD
	Amplifier	Gali-21+	Mini-Circuits
	Amplifier	Gali-84	Mini-Circuits
	Attenuators	DAT-15R5-SN	Mini-Circuits
	RF-switch	HMC284MS8G	Hittite Microwave Corp.
	Mixer	SYM25-DHW	Mini-Circuits
	Filter amplifier	ADA4817 (single-ended)	Analog Devices
	Filter amplifier	ADA4932-1 (balanced)	Analog Devices
Digital board	Shift-register	MC10EP142MNG	ON Semiconductors
	VCO	ROS-2082-119+	Mini-Circuits
	Synthesizer	ADF4106	Analog Devices
	Crystal	5597ASX3SVT	European Crystal Org.
	ECL clock splitter	ADCLK925	Analog Devices
	Amplifier	Gali-21+	Mini-Circuits
	CPLD	EPM570T144	Altera

4. DIGITAL BOARD

The choice of the periodic functions $p_i(t)$ dictates the Nyquist rate of the input signals that the MWC can handle. In particular, if $p_i(t)$ has Fourier coefficients c_{il} with non-negligible amplitudes for all $0 \le l \le L$, then the MWC can capture signals with band locations anywhere below Lf_p, corresponding to a Nyquist rate of $2Lf_p$. The precise requirement on the magnitude of c_{il} depends on the properties of the digital reconstruction algorithm and is beyond the current scope [1]. Nonetheless, in principle, every periodic function with high-speed transitions within the period T_p can be appropriate. The digital board in our design realizes a sign-alternating function, with M sign intervals within the period T_p. The choice $M \approx f_{\text{NYQ}}/B$ was proposed in [1] and analyzed in [7]. In the sequel, we elaborate on the circuit work that ensures the periodicity of $p_i(t)$ and explain the choice of the sign pattern. Other design aspects are detailed in the technical report [9].

4.1. Periodicity and high-speed alternations

A straightforward approach to realize a ± 1 logic waveform would be to program the desired pattern into a field programmable gate array (FPGA) device. Unfortunately, this approach is not suited for realizing a high-rate SR. Popular FPGA devices do not stand a clock rate of 2.075 GHz and premium devices are power consuming and very expensive. Therefore, we had to depart from conventional logic design and realize the SR using discrete devices.

The difficulty in implementing a discrete SR at 2.075 GHz is in satisfying the setup/hold timing constraints. For correct functionality, the data must propagate between the flops sufficiently fast and accurate before the next clock edge arrives. Any solution which is based on fine tuning of short time delays (on the order of $1/2.075 \approx 480$ picosecs) is prone to errors; the wide literature on time mismatches in interleaved-ADCs is evidence to this difficulty, cf. [10]. To overcome this challenge, our design is based on the MC10EP142MNG device, which implements an internally-wired 8 bits SR in ECL technology. We exploited a specific property of that device. The datasheet reports on a maximal shifting frequency of 2.8 GHz (equivalent to a minimal clock period of 357 picosecs), and a delay from clock to output of about 670 picosecs. The meaning is that the manufacturer guarantees correct functionality in the internal register, up to a shifting rate of 2.8 GHz, though once the signal leaves the device the delay is almost doubled.

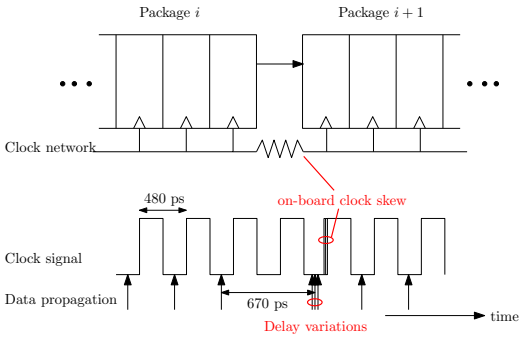

Fig. 6: The interface of adjacent SR packages involves uncertainty on the clock network due to on-board routing. The timing diagram illustrates the propagation of data in the SR chain. Setup and hold constraints are satisfied internally by manufacturer, and externally by viewing the clock to output delay as an additional flop in between adjacent packages.

Capitalizing on this difference is the key for satisfying the setup and hold requirements with no additional hardware. As illustrated in Fig. 6, since the delay of the last bit in each package is larger than the clock period, it reaches the next package one clock later than what would be normally expected in a standard FPGA design. This behavior seems erroneous and is likely to be reported as a violation of timing constraints by software tools. Fortunately, it follows from Fig. 6 that we can view the large delay as an additional flop in between adjacent packages, with an equivalent clock-to-output delay of 670-480 = 190 picosecs. In other words, the data arrives about half a clock period before the next edge, in which case both the setup and time requirements are satisfied. To emphasize, the proposed solution requires no time-delay elements or synchronization mechanisms whatsoever. This allows a sign pattern of length $M = 108$ bits to be realized by only 96 physical flops.

To verify the periodicity of the mixing waveforms, we observed the outputs of the digital board in a spectrum analyzer. Fig. 7(a) depicts the spectrum of $p_i(t)$, which consists of equalispaced Diracs, namely highly concentrated energy peaks, as expected for periodic waveforms. The spacing between the Diracs was measured as 19.212 MHz, validating the design choice of f_p in Table 1. The Dirac spectral lines appear steady, ensuring the periodicity of $p_i(t)$.

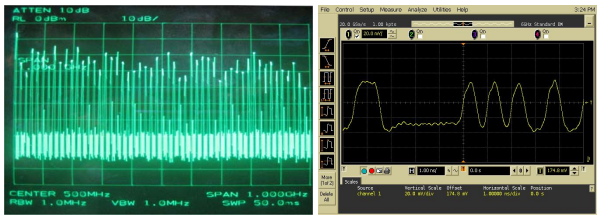

(a) (b)

Fig. 7: The spectrum of a sign-alternating periodic waveform (a), and the time-domain appearance (b).

The time-domain appearance of $p_i(t)$ is plotted in Fig. 7(b), showing sign alternations that are far from rectangular transitions on the Nyquist grid. Fortunately, since periodicity is the only essential requirement of the MWC, the nonideal time-domain appearance has no effect in practice.

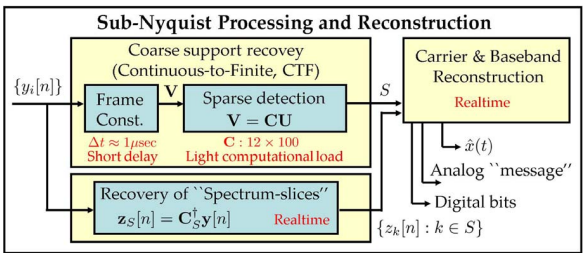

Fig. 8: Block diagram of the reconstruction algorithm [1].

4.2. Sign-pattern selection

The SR of the digital board is programmed to the initial value

$$\text{Pattern} = \text{43 A7 A5 D7 96 AB 62 B7 2A B3 5C AC}, \quad (5)$$

encoded in hexadecimal bytes. The study in [7] introduced a theoretical measure, termed the expected restricted isometry property (ExRIP), for the quality of a given set of periodic sign-alternating functions $p_i(t)$. Among the conclusions of [7] is that Gold, Kasami, and even randomly-chosen binary patterns are suitable for the MWC system, whereas orthogonal Hadamard sequences are inadequate. We therefore generated a set of candidate patterns with high ExRIP qualities. In order to choose between these patterns, we observed $p_i(t)$ in a spectrum analyzer and decided on (5) since the power of its coefficients c_{il} were relatively balanced, as depicted in Fig. 7(a). Such a balance ensures approximately equal power levels for the multiple sinusoids comprising $p_i(t)$. Experimentally, we noticed that a balanced Dirac set contributes to mitigating nonlinear distortions in the nonordinary mixing.

5. SUB-NYQUIST DEMONSTRATION

In this section, we demonstrate sub-Nyquist sampling and reconstruction using our designed system. For the paper to be self-contained, we first briefly outline the steps of the digital recovery algorithm.

5.1. Background: Reconstruction algorithm

The heart of the reconstruction algorithm is a block, named continuous to finite (CTF), which collects samples $y_i[n]$ over a short time duration and constructs a finite-dimensional optimization program from these samples [1, 6]. As is depicted in Fig. 8, the samples are collected into a frame matrix $\mathbf{V}$. The optimization targets at a matrix $\mathbf{U}$, satisfying $\mathbf{V} = \mathbf{CU}$ for $\mathbf{C} = \{c_{il}\}$, such that $\mathbf{U}$ has the minimal number of non-identically zero rows. This type of optimization got an extensive treatment in the compressed sensing literature, with plenty of off-the-shelf solvers, any of which can be utilized in the recovery scheme of Fig. 8; example techniques include ℓ_1 minimization and greedy-type algorithms [11]. The gist of the recovery flow is that $\mathbf{U}$ (which solves a finite-dimensional program) indicates the set S of active spectrum slices (of a continuous signal), namely the indices of the f_p-width spectrum slices that contain signal energy. Once the active slices are detected, their content is reconstructed in realtime, including recovering the unknown carrier of each transmission and the information it encodes [2]. Together, the digital processing blocks of Fig. 8 provide a seamless interface to standard DSP packages.

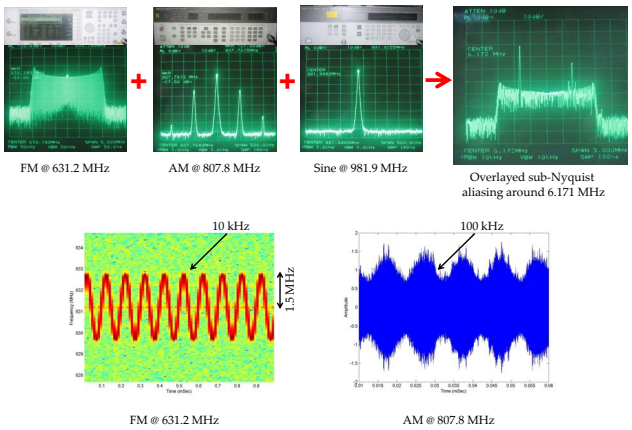

Fig. 9: Three signal generators are combined at the system input terminal. The spectrum of the aliased image (first channel) shows overlapped aliasing at baseband. The recovery algorithm estimates the correct carriers and reconstructs the original individual signals.

5.2. Signal reconstruction

In order to prove the sub-Nyquist sampling capability of our design, three signal were combined at the input terminal of the MWC prototype: an amplitude-modulated (AM) signal at 807.8 MHz with 100 kHz envelope, a frequency-modulation (FM) source at 631.2 MHz with 1.5 MHz deviation at 10 kHz rate and a pure sine waveform at 981.9 MHz. The carrier positions were chosen so that their aliases overlay at baseband, as the photos in Fig. 8 demonstrate. Despite the interfering energies in $y_i[n]$, the digital recovery algorithm detected the correct support set S (CTF) successfully . The carrier positions were estimated up to 50 kHz accuracy. In addition, the figure affirms correct reconstruction of the AM and FM signal contents. Documentation and video recording are available online on our websites [3].

6. CONCLUSIONS

We presented a circuit realization of the modulated wideband converter – a sub-Nyquist sampler. Our design can handle wideband inputs and sample them at a fraction of the Nyquist rate. We have chosen to implement a specific configuration of the converter, in which the Nyquist rate of the input is around 2 GHz and the spectrum occupancy reaches 120 MHz. The sampling rate is as low as 280 MHz, which approaches the lowest possible rate for multiband signals with unknown carrier positions.

In addition to presenting the sub-Nyquist sampler, we put an emphasis on two circuit challenges: mixing a signal with multiple sinusoids and generating periodic waveforms with transients on the order of the Nyquist interval. In order to achieve the desired effects, we employed standard devices, modified their specifications due to the nonordinary usage and added auxiliary circuitry accordingly. Further investigation of these circuit structures, beyond the current application of sub-Nyquist sampling, may assist in developing alternative solutions for these tasks.

State-of-the-art sub-Nyquist methods were theoretically compared in [2], within a general framework for sub-Nyquist ADC, termed Xampling. The MWC was found superior over the alternatives in terms of hardware and software complexities. Of the existing theoretical methods, we point out two approaches with hardware implementation. A hardware realization of the random demodulator was demonstrated in [12] for a 800 kHz Nyquist-rate input and 100 kHz sampling rate. The digital reconstruction was carried out by a 160 MHz processor. The Nyquist folding system of [13] utilizes nonlinear effects to smear a narrowband transmission. Reconstruction proof, in particular to the typical scenario of overlaps in baseband, as we exemplify for the MWC in Fig. 9, was not published so far. To the best of our knowledge, this paper is the first to present a wideband hardware of a sub-Nyquist system.

7. REFERENCES

[1] M. Mishali and Y. C. Eldar, "From theory to practice: Sub-Nyquist sampling of sparse wideband analog signals," *IEEE J. Sel. Topics Signal Process.*, vol. 4, no. 2, pp. 375–391, Apr. 2010.

[2] M. Mishali, Y. C. Eldar, and A. Elron, "Xampling: Signal acquisition and processing in union of subspaces," *CCIT Report no. 747, EE Dept., Technion; arXiv.org 0911.0519*, Oct. 2009.

[3] M. Mishali and Y. C. Eldar, "The modulated wideband converter: Hardware experiments," available: http://www.technion.ac.il/~moshiko/hardware.html.

[4] Y.-P. Lin and P. P. Vaidyanathan, "Periodically nonuniform sampling of bandpass signals," *IEEE Trans. Circuits Syst. II*, vol. 45, no. 3, pp. 340–351, Mar. 1998.

[5] C. Herley and P. W. Wong, "Minimum rate sampling and reconstruction of signals with arbitrary frequency support," *IEEE Trans. Inf. Theory*, vol. 45, no. 5, pp. 1555–1564, Jul. 1999.

[6] M. Mishali and Y. C. Eldar, "Blind multi-band signal reconstruction: Compressed sensing for analog signals," *IEEE Trans. Signal Process.*, vol. 57, no. 3, pp. 993–1009, Mar. 2009.

[7] ——, "Expected-RIP: Conditioning of the modulated wideband converter," in *Information Theory Workshop, 2009. ITW 2009. IEEE*, Oct. 2009, pp. 343–347.

[8] Y. Chen, M. Mishali, Y. C. Eldar, and A. O. Hero III, "Modulated wideband converter with non-ideal lowpass filters," in *ICASSP 2010*, 2010, pp. 3630–3633.

[9] M. Mishali, Y. C. Eldar, O. Dounaevsky, and E. Shoshan, "Xampling: Analog to digital at sub-Nyquist rates," *arXiv.org 0912.2495; to appear in Circuits, Devices & Systems, IET*.

[10] P. Nikaeen and B. Murmann, "Digital compensation of dynamic acquisition errors at the front-end of high-performance A/D converters," *IEEE Trans. Signal Process.*, vol. 3, no. 3, pp. 499–508, Jun. 2009.

[11] J. A. Tropp, "Algorithms for simultaneous sparse approximation. Part I: Greedy pursuit," *Signal Process. (Special Issue on Sparse Approximations in Signal and Image Processing)*, vol. 86, pp. 572–588, Apr. 2006.

[12] T. Ragheb, J. N. Laska, H. Nejati, S. Kirolos, R. G. Baraniuk, and Y. Massoud, "A prototype hardware for random demodulation based compressive analog-to-digital conversion," in *Circuits and Systems, 2008. MWSCAS 2008. 51st Midwest Symposium on*, 2008, pp. 37–40.

[13] G. L. Fudge, R. E. Bland, M. A. Chivers, S. Ravindran, J. Haupt, and P. E. Pace, "A Nyquist folding analog-to-information receiver," in *Proc. 42nd Asilomar Conf. on Signals, Systems and Computers*, Oct. 2008, pp. 541–545.